Adaptive DC Voltage Control for Single-phase Hybrid Filter with PV Integration Capability

ChenPei Zheng[1], NingYi Dai[1], ManChung Wong[1], ChiKong Wong[1] and Miao Zhu[2]
[1] Department of Electrical and Computer Engineering, University of Macau, Macau, P. R. China
[2] Department of Electrical Engineering, Shanghai Jiao Tong University, Shanghai, China

***Abstract*-- The operational voltage of the hybrid power filter (HPF) is much lower than an active power filter (APF) when reactive power of inductive loads is compensated. The active power transfer capability of the HPF is utilized to achieve PV generator integration in this paper. The proposed system is a low cost solution for power quality conditioning and PV integration in modern buildings. The low dc voltage reduces the energy stored in the dc capacitor and is safer for building-integrated PV systems. In order to reduce switching loss and switching noises, an adaptive dc voltage controller is proposed. The dc-link voltage as well as the power flow controllable range of the HPF is adaptively changed according to different loading and PV generator output. Simulation and experimental results are provided to show the effectiveness of the adaptive dc voltage control method.**

***Index Terms*—Adaptive dc voltage control, hybrid power filter, power quality, PV integration.**

I. INTRODUCTION

With increasing concerns about energy saving technology and rapid development of power electronics, the renewable energy sources(RES) have been integrated into the microgrid on a large scale [1][2]. Photovoltaic (PV) power has been a promising renewable energy source due to its ability to operate with much less restriction on location, and ease of maintenance [3][4]. Building-integrated PV electric power systems are becoming popular recently. A parallel-connected inverter is required to integrate the PV generation system to the power gird. This parallel-connected inverter may also serve as reactive power or harmonic compensator in some applications[5][6]. However, the operational voltage of this inverter is high since its topology is similar to a conventional APF [7][8].

At the same time, more energe saving loads are put into use in modern buildings, more concerns are paid to distribution system power quality. Power filters are applied to enhance the distribution system power quality and to reduce the operational losses. Hybrid power filter (HPF) was proposed for achieving the reactive power and harmonic compesation in a more economical way [9][10]. In one of the widely used hybrid filter topology, a passive filter is connected in series with an active power filter (APF)[11]. The system fundamental voltage is dropped across the coupling capacitance but not the active power filter part[12]. The system cost is reduced since the dc-link operating voltage of the inverter is much lower [13][14].

In this paper, the PV integration capability of the single-phase HPF is investigated. The DC bus of the HPF is connected to the output of a PV generation system via a boost-half-bridge dc/dc converter. The HPF transfers the active power from the PV generators to the power grid. At the same time, the reactive power compensation capability are not affected. The dc-link operating voltage of the HPF can be set much lower than an APF or a grid-connected inverter for PV generators [15][16][17].

In contract with the active power filter, the operational voltage of the HPF may vary is a wide range with the power to be controlled. To fix the dc voltage may introduce the problem of high switching noises and output waveform distortion. An adaptive dc voltage controller was used in a three-phase hybrid filter, in which the dc voltage is adjusted according to load reactive power [18]. In this paper, the dc voltage of the HPF is determined by load reactive power as well as active power from PV generator. An adaptive dc control considering active and reactive power simultaneously will be studied.

In Section II, the system configuration and control system is introduced. The proposed adaptive dc voltage control method is discussed in Section III. The simulation results are given in Section IV and experimental results are given in Section V.

II. SYSTEM CONFIGURATION AND CONTROL SYSTEM

A. System configuration

The system configuration of the HPF connecting a PV generator is shown in Fig.1. The output of the PV generator connects to a boost-half-bridge dc-dc converter. The maximum power point tracking (MPPT) is achieved by controlling this dc-dc converter. The high-frequency transformer achieves galvonic isolation. The output of the dc-dc converter is connected to the dc bus of the HPF.

The HPF is connected to the point of common coupling (PCC) via a capacitor in series with an inductor. The impedance of the coupling branch is express as:

$$Z = -j\frac{1}{\omega C_C} + j\omega L_C = -jX_C \tag{1}$$

In order to reduce the operational voltage of the inverter, the total impedance of the coupling branch is capacitive. It is selected according to the average reactive power being consumed by the loads at the PCC.

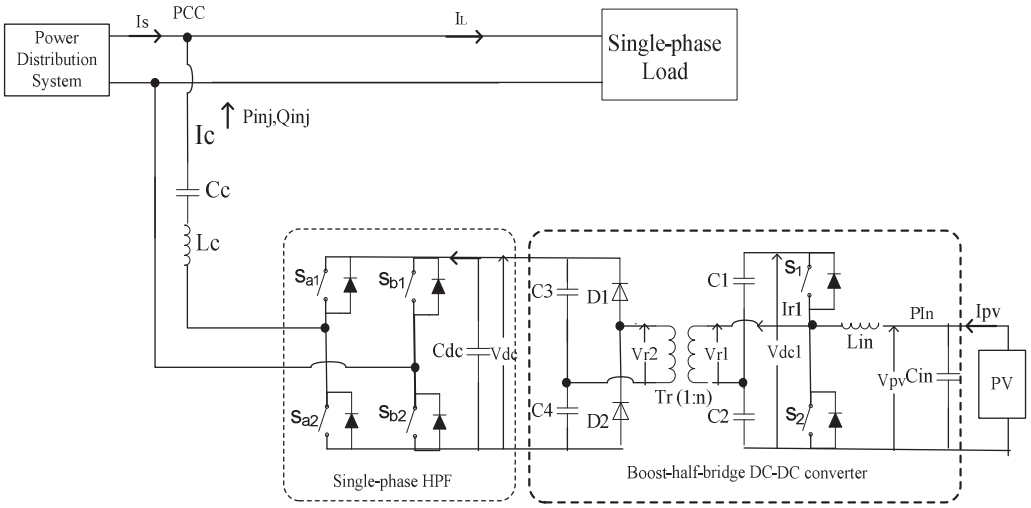

Fig. 1 System Configuration of the hybrid power filter connecting a PV generator

The operational voltage is kept low when inductive loads are compensated by the HPF. Since a PV generation system is connected, the HPF also transfers active power to the grid. The active and reactive power injecting to the PCC are expressed as:

$$P_{inj} = \left(\frac{V_s V_{inv}}{Xc}\cos\delta - \frac{V_s^2}{Xc}\right)\cos\theta + \frac{V_s V_{inv}}{Xc}\sin\delta \cdot \sin\theta \quad (2)$$

$$Q_{inj} = \left(\frac{V_s V_{inv}}{Xc}\cos\delta - \frac{V_s^2}{Xc}\right)\sin\theta - \frac{V_s V_{inv}}{Xc}\sin\delta \cdot \cos\theta \quad (3)$$

where V_{inv} and δ are the root mean square (RMS) value and phase angle of operational voltage of the inverter; Xc and θ are the amplitude and phase angle of the coupling impedance. θ equals to -90 degree according to (1). By combining (2) and (3), the amplitue of operational voltage of the inverter is expressed as [10]:

$$V_{inv} = V_s\sqrt{(1-\frac{Q_{inj}}{S_{base}})^2 + (\frac{P_{inj}}{S_{base}})^2} \quad (4)$$

where $S_{base} = V^2 / X_C$ (5)

The power base in (5) is used to normalize the active and reactive power injecting to the grid, so that the expression in (4) is simplified. The dc voltage of the inverter needs to be higher than the peak value of its operational voltage, otherwise the output waveform is distorted due to overmodulation. Hence, the dc voltage is calculated as follows, in which a coefficient M is added to provide a safe margin.

$$V_{dc} = \sqrt{2}\cdot M \cdot V_s\sqrt{(1-\frac{Q_{inj}}{S_{base}})^2 + (\frac{P_{inj}}{S_{base}})^2} \quad (6)$$

The variation of dc voltage with active and reactive power flow is shown in Fig.2. It is concluded from Fig. 2 that the dc voltage is lower when the reactive power locates in the vicinity of the power base. Hence, the HPF fit to be used in applications which load reactive power vary in a narrow range at the PCC. The capacity of the PV generation system connecting to the HPF is also limited. It is better to be lower than half of the power base. Under this situation, the operational voltage of the HPF can be kept lower than grid side voltage. Hence, the dc bus voltage of this system is much lower than that of a conventional PV integration inverter or active power filter.

B. Control system

The control system of the HPF connecting a PV generator is provided in Fig. 3. It is constructed by two main blocks. One is mainly for controlling the dc-dc converter. In order to increase the efficiency of the PV generator, the gradient approximation method is used to achieve maximum power point tracking (MPPT). The detailed description of implementing the MPPT control in a boost-half-bridge dc-dc converter was given in [19][20].

The second block is used to control the HPF. The load reactive power is calculated by instantaneous reactive power theory. The active power is calculated by multiplying output voltage and current of the PV module. The dc-link voltage regulator is implemented by a PI regulator. The output of the PI controller is fed back to both active and reactive power reference in order to adjust the dc bus voltage to the set reference value.

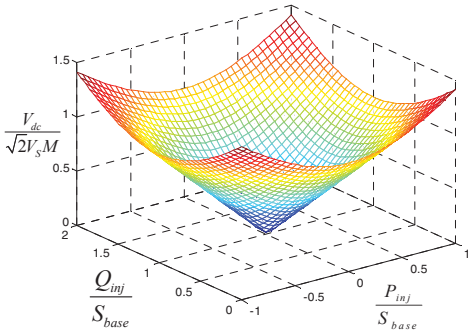

Fig.2 Variation of dc voltage with active and reactive power

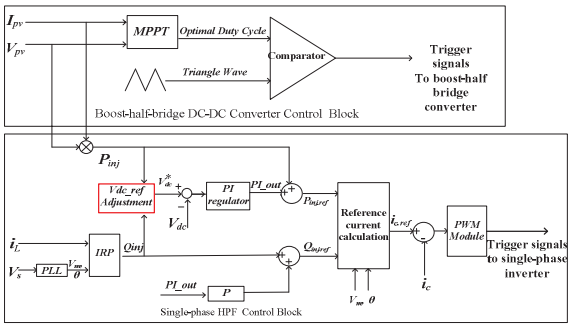

Fig.3 Control system block diagram

When the HPF operates, the active power from the PV generators is injected to the grid and reactive power is provided to improve power factor at the PCC. Both these two functions can improve the energy efficiency in a distribution system. The dc voltage reference is got from a V_{dc_ref} adjustment module, which is marked in red in Fig.3. This module is proposed to improve the efficiency and reduce the output current ripple, which will be discussed in detail in next Section.

III. Adaptive DC Voltage Control of the HPF

The dc voltage of the inverter is calculated by using of active and reactive power to be transferred, as illustrated in (6). The maximum active power is determined by the capacity of PV generation system. It is denoted by P_{max}. The reactive power variation range is determined by the loads connecting to the PCC. The maximum dc voltage is calculated by (7).

$$V_{dc.max} = \sqrt{2} \cdot M \cdot V_s \sqrt{(\frac{Q_{range}}{2})^2 + (\frac{P_{max}}{S_{base}})^2} \quad (7)$$

where $Q_{range} = (Q_{inj.\max} - Q_{inj.\min}) / S_{base}$.

Fig.4 illustrates the relationship between the dc voltage and power control range. The radius of each red circle corresponds to an operational voltage of the inverter. With the active and reactive power to be transferred, the operational point of the HPF is located on the plane with the coordinates (P_{inj}, Q_{inj}).

As shown in Fig.2, the dc voltage varies in a wide range with active and reactive power. Instead of using the maximum dc voltage in (7), a lower dc voltage can be used if the operational points locate in the vicinity of the point *O* in Fig.4. At point *O*, the active power is zero and reactive power equals to S_{base}. When the single-phase inverter operates to give the same output voltage, a lower dc bus voltage means less energy is stored in its dc bus. The voltage stress on each power switch is also reduced. With a modulation index close to one, the output waveform distortion can also be reduced by properly implementing the pulse width modulation (PWM) unit.

Therefore, an adaptive dc voltage control block is proposed for the single-phase HPF with PV integration capability. It is used to adjust dc voltage according to active and reactive power to be transferred. The dc voltage reference can be calculated by (6) according to real-time power variations. However, this method will cause frequent change of the dc reference. Not only dc fluctuation problem, but power control accuracy will be affected. A more practical solution is to classify the reference dc voltage into *n* levels: $V_{dc.L1}, V_{dc.L2} \cdots V_{dc.\max}$ ($V_{dc.L1} < V_{dc.L2} \cdots < V_{dc.\max}$). The voltage of each level is expressed as:

$$V_{dc.Lk} = \frac{k}{n} \cdot V_{dc.max} \quad (8)$$

where *k= 1, 2, ... (n-1)*.

For each dc voltage obtained from (6), it is rounded to the closest up level. The dc voltage at this level is the final dc reference V_{dc}^* sending to the dc control block, as shown in Fig.3. In this way, the dc voltage is kept at a stable value within a specific compensation range. The range is a ring bounded by two neighboring dc voltage level, as illustrated in Fig. 4. The dc voltage selection process is given in Fig.5. When the V_{dc} is less than the lowest dc voltage level $V_{dc.L1}$, the dc voltage reference is $V_{dc}^* = V_{dcL1}$. If not, dc selection process will go on until V_{dc} is found to be less than one pre-defined dc voltage level. The maximum power flow controllable range is reached when the dc-link voltage of HPF reaches $V_{dc.max}$.

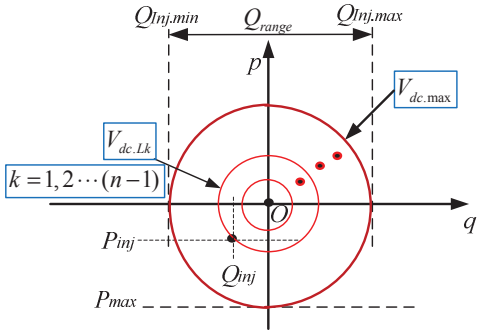

Fig.4 Adaptive dc voltage control

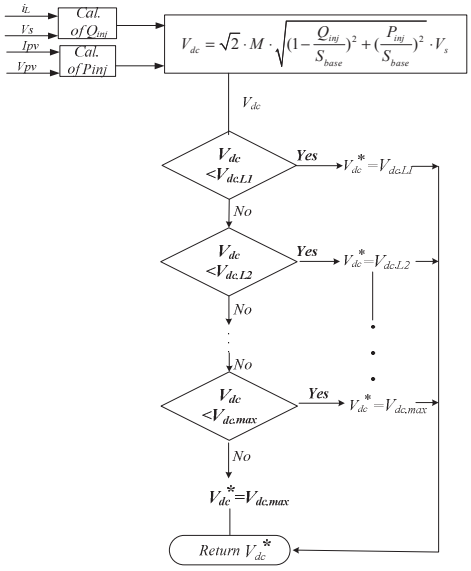

Fig.5 Adaptive dc voltage selection flow chart

The dc voltage adjustment block in Fig.3 is implemented based on the adaptive dc voltage selection flow chart in Fig. 6. The dc bus voltage of the HPF changes as the active and reactive power to be controlled vary.

IV. Simulation Results

Simulation verifications are carried out in PSCAD/EMTDC. The system configuration is shown in Fig.1.The system parameters in simulation are given in Table I. In simulation, the loads are modeled by a series-connected branch of an inductor and a resistor. The load and PV module setting are given in Table II. The system operates under case 1 until 2s, and then it is shifted to the settings in case 2 during 2s to 3s. The active and reactive power need to be controlled by the HPF is listed in Table II. As active and reactive power changes, the calculated dc voltage and the final selected dc voltage reference l are also listed in Table II.

The HPF is controlled to achieve active power injection and reactive power compensation simultaneously. Both fixed dc voltage control method and the proposed adaptive dc voltage control method is implemented. Simulation results are given in Figs. 5. V_{dc} represents the dc voltage. I_{load}, I_s is the load current and source current respectively. *Ic* is the output current of the HPF. The system performance indexes are summarized in Table III and IV. Results indicate that the HPF achieves active power transfer and reactive power compensation simultaneously with the two control methods.

The dynamic process is shown in Fig. 6 when the system is shifted from setting in case 1 to case 2. The dc voltage is kept at 105V with fixed dc voltage control. The dc voltage is smoothly changed from 105V to 90V when the system operate from under case 1 to under case 2 with the proposed adaptive dc votlage control. The system performance is kept almost the same but the dc voltage is reduced by using the proposed method. The output current distortion is also slghtly reduced.

TABLE I System parameters in simulation

Grid voltage V_s	*220 V*
Filter inductor L_{PF}	*7.5mH*
Filter capacitor C_{PF}	*54 uF*
Dc-link capacitor	*6.0mF*
Power basement S_{base}	*820 VA*

TABLE III Comparisons in simulation under case 1

Performance Indexes	Loading Side	Source Side	
	Case 1	*Fixed dc voltage control*	*Adaptive dc voltage control*
Active power	846W	774W	773W
Reactive power	591Var	-18Var	-16Var
Power Factor	0.82	1.00	1.00
Current RMS	4.69A	3.51A	3.55A
Current THD	/	3.21%	3.23%
P_{inj}	/	72W	73W
Q_{inj}	/	609Var	607Var

TABLE IV Comparisons in simulation under Case2

Performance Indexes	Loading Side	Source Side	
	Case 2	*Fixed dc voltage control*	*Adaptive dc voltage control*
Active power	940W	883W	881W
Reactive power	656Var	-10Var	-14Var
Power Factor	0.82	1.00	1.00
Current RMS	5.23A	4.06A	3.98A
Current THD	/	1.91%	1.75%
P_{inj}	/	57W	59W
Q_{inj}	/	666Var	670Var

V. . Experimental Results

In order to verify the effectiveness of the proposed adaptive dc voltage control for the HPF with PV integration capability, hardware verifications are carried out. A small capacity prototype was built and tested. The PV module and dc-dc converter is replaced by an ac source connecting a rectifier. Table V illustrates the system parameters in the experiment. The load reactive power and active power from the external sources in experiment are listed in Table VI. The selected dc voltage is also given in Table VI.

The fixed dc voltage control and adaptive dc voltage control are both implemented and tested in experiment. The experimental results are given in Figs. 7 and 8. The HPF is able to compensate load reactive power and transfer active power simultaneously. Its dc voltage is much lower than the grid side system voltage. Under the case 2, the dc voltage is adjusted to 30V by using the proposed adaptive dc voltage control. The system performance is kept almost the same, but dc voltage is only 75% of that required under fixed dc voltage control. The system performance in experiment are summarized in Table VII and Table VIII for comparison. The effectiveness of the proposed control method is shown with the experimental results.

TABLE V System parameters in the experiment

Grid voltage V_s	*55 Vrms*
Filter inductor L_{PF}	*130 uF*
Filter capacitor C_{PF}	*3 mH*
Dc-link capacitor	*10mF*
Power basement S_{base}	*130 VA*

TABLE VII Comparisons of the experiment results in Case1

Performance Indexes	Loading Side	Source Side	
	Case 1	*Fixed dc voltage control*	*Adaptive dc voltage control*
Active power	129W	109W	108W
Reactive power	81Var	7Var	12Var
Power Factor	0.84	0.99	0.99
Current RMS	2.67A	1.93A	1.92A
Current THD	/	7.4%	6.6%
P_{inj}	/	20W	21W
Q_{inj}	/	74Var	69Var

TABLE II LOADING AND PV MODULE SETTING IN SIMULATION

	Cases	*Loading Parameter*		*PV module setting*	Q_L	P_{source}	V_{dc_min}	V_{dc}^*
Fixed DC Control Method	**Case 1** [0.0s-2.0s]	1st loading	L_1=85.4mH R_1=38.4Ω;	21w/m^2,28° C	591Var	75W	93V	105V
	Case 2 [2.0s-3.0s]	2nd loading	L_2=76.9mH; R_2=34.6Ω;	19w/m^2,28° C	656Var	60W	76V	105V
Adaptive DC Control Method	**Case 1** [0.0s-2.0s]	1st loading	L_1=85.4mH R_1=38.4Ω;	21w/m^2,28° C	591Var	75W	93V	105V
	Case 2 [2.0s-3.0s]	2nd loading	L_2=76.9mH; R_2=34.6Ω;	19w/m^2,28° C	656Var	60W	76V	90V

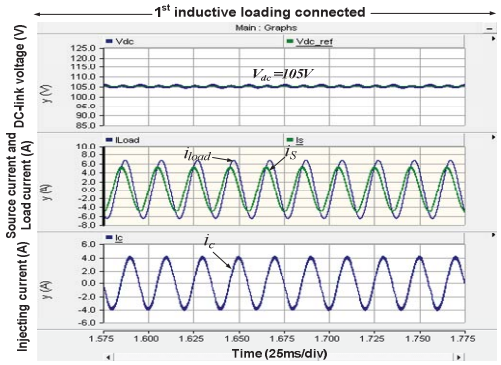

DC voltage and Current waveform in Case 1

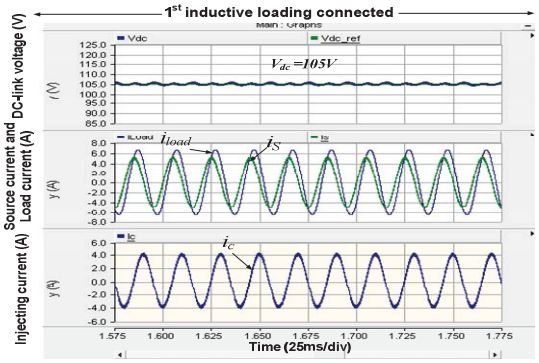

DC voltage and Current waveform in Case 1

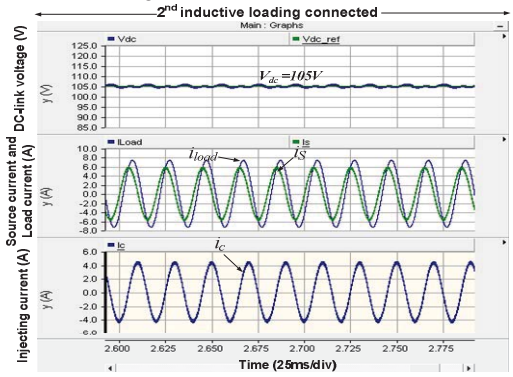

DC voltage and Current waveform in Case 2

(a)

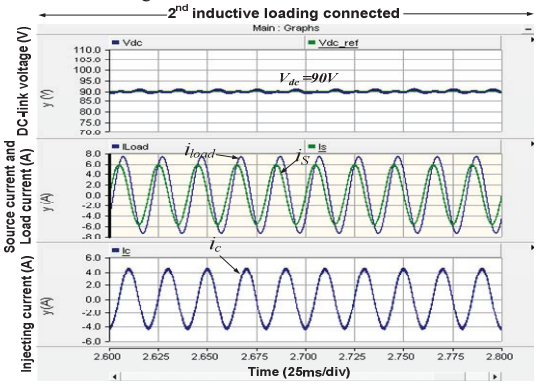

DC voltage and Current waveform in Case 2

(b)

Fig.5 Comparisons of dc voltage and the current waveforms (a) fixed dc-link voltage control (b) adaptive dc-link voltage control

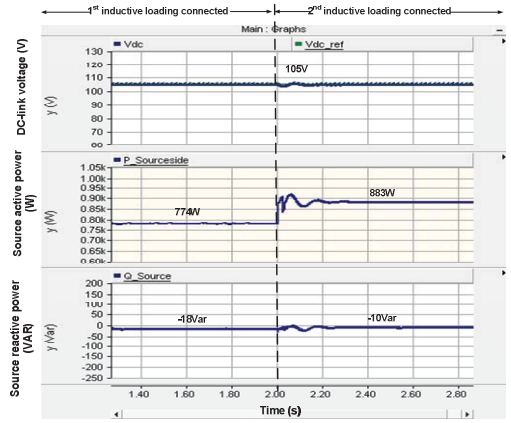

(a)

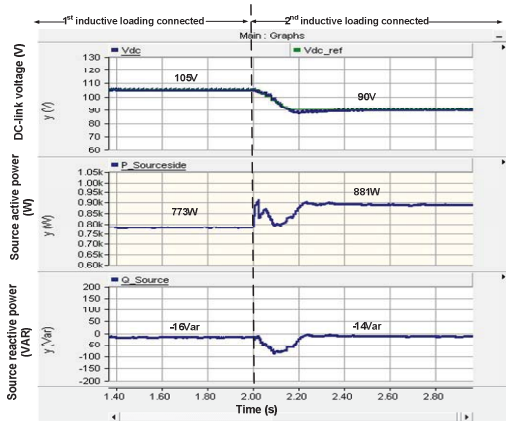

(b)

Fig.6 Comparison during dynamic process (a) fixed dc-link voltage control (b) adaptive dc-link voltage control

TABLE VI THE DC-LINK VOLTAGE LEVEL WITH RESPECT TO Q_L AND P_{source} IN DIFFERENT STAGES FOR DIFFERENT METHODS.

	Cases	*Loading Parameter*		Q_L	P_{source}	V_{dc_min}	V_{dc}^*
Fixed DC Control Method	**Case 1** [0s-160s]	1st loading	L_1=32.82mH R_1=16.97Ω;	81Var	20W	38V	40V
	Case 2 [160s-240s]	2nd loading	L_2=30.13mH; R_2=15.02Ω;	90Var	10W	28V	40V
Adaptive DC Control Method	**Case 1** [0s-160s]	1st loading	L_1=32.82mH R_1=16.97Ω;	81Var	20W	38V	40V
	Case 2 [160s-240s]	2nd loading	L_2=30.13mH; R_2=15.02Ω;	90Var	10W	28V	30V

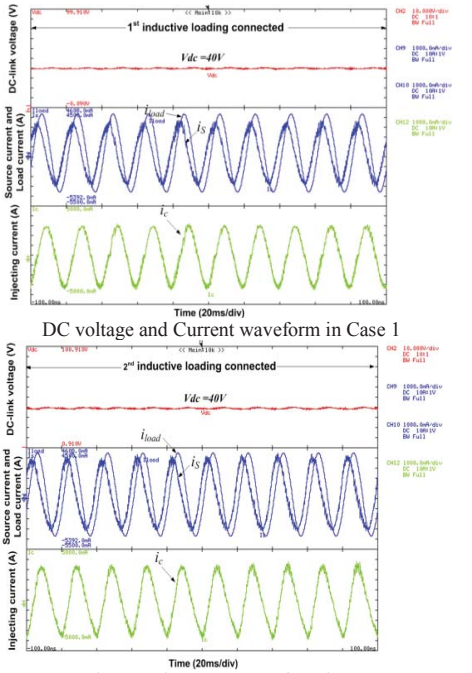

DC voltage and Current waveform in Case 1

DC voltage and Current waveform in Case 2

(a)

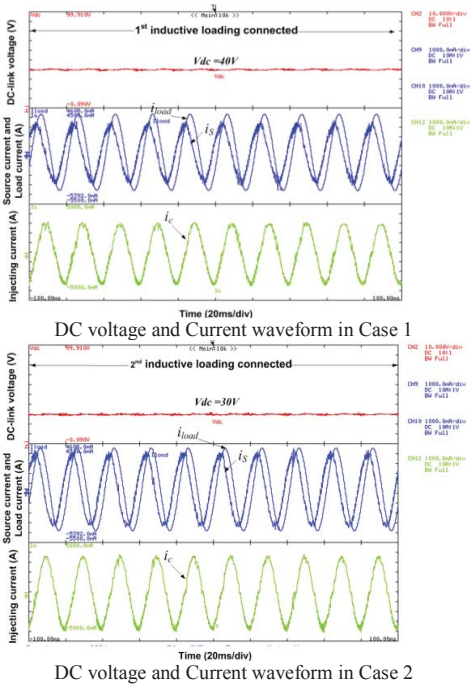

DC voltage and Current waveform in Case 1

DC voltage and Current waveform in Case 2

(b)

Fig.7 Comparisons of dc voltage and the current waveforms (a) fixed dc-link voltage control (b) adaptive dc-link voltage control

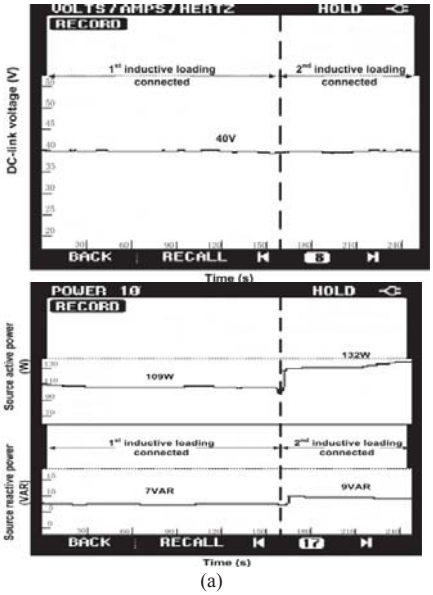

(a)

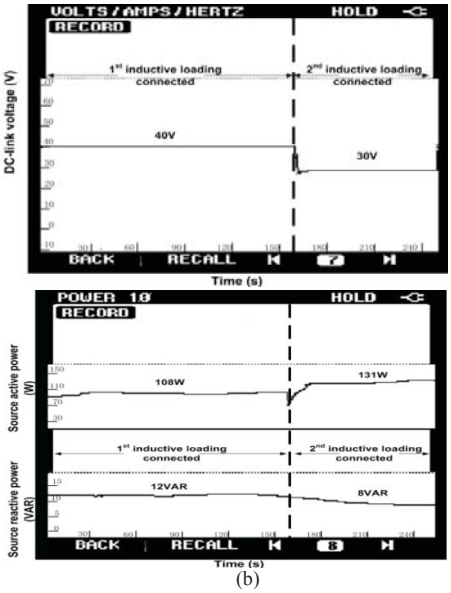

(b)

Fig.8 Comparison during dynamic process (a) fixed dc-link voltage control (b) adaptive dc-link voltage control

TABLE VIII COMPARISONS OF THE EXPERIMENT RESULTS IN CASE 2

Performance Indexes	Loading Side	Source Side	
	Case 2	*Fixed dc voltage control*	*Adaptive dc voltage control*
Active power	140W	132W	131W
Reactive power	90Var	9Var	8Var
Power Factor	0.84	0.99	0.99
Current RMS	2.93A	2.38A	2.21A
Current THD	/	7.1%	6.4%
P_{inj}	/	8W	9W
Q_{inj}	/	81Var	82Var

VI. CONCLUSIONS

In this paper, a HPF with PV integration capability is studied. It is a low cost solution for power quality conditioning and PV integration in modern buildings, since its operational voltage is lower than the grid voltage. The low dc bus voltage reduces the energy stored in the dc capacitor and is safer for building integrated PV systems. An adaptive dc voltage control method is proposed, in which both dc voltage and power flow control capability of the HPF are dynamically adjusted according to different operation modes. The validity of the proposed method is verified by both simulation and experimental results.

ACKNOWLEDGMENT

The authors would like to thank the Science and Technology Development Fund, Macao SAR Government with the project (072/2012/A3) and University of Macau with the project (MYRG2015-00084-FST) for their financial support.

.

REFERENCES

[1] Xiang Yuan, ZhenXing Qian, Yang Zhou, "Discussion on the development trend of smart grid and its key technology" *2012 China International Conference on Electricity Distribution*, 5-6 Sep. 2012,pp.5-6.

[2] F. Blaabjerg. "Overview of Control and Grid Synchronization for Distributed Power Generation Systems", *IEEE Trans. Ind. Electron*, vol.53, no.5, pp. 1398-1409, Oct. 2006.

[3] M. J. V. Vazquez, J. M A. Marquez, and F. S. Manzano, "A methodology for optimizing stand-alone PV-System sizing using parallel-connected dc/dc converter," I*EEE Trans. Ind. Electron.*, vol. 55, no. 7, pp. 2664–2673, Jul. 2008.

[4] T. Kerekes, R, Teodorescu, M. Liserre, C. Klumpner, and M. Sumner, "Evaluation of three-phase transformerless photovoltaic inverter topologies," *IEEE Trans. Power Electron.*, vol. 24, no. 9, pp. 2202–2211, Sep.2009.

[5] Jiefeng Hu, Jianguo Zhu and Dorrel, D. G., "Model prediction control of grid-connected inverters for PV systems with flexible power regulation and switching frequency reduction", *IEEE Trans. Ind. Applica*., vol.51, no.1, pp. 587-594, Jan. 2015.

[6] Zhang, Li, Kai Sun, Yan Xing, Lanlan Feng,and Hongjuan Ge. "A Modular Grid- Connected Photovoltaic Generation System Based on DC Bus", *IEEE Trans. Power Electron*, vol.26, no.2, pp. 523-531, 2011.

[7] S. H. Hwang, L. Liu, H. Li, and J. M. Kim, "DC offset error compensation for synchronous reference frame PLL in single-phase grid-connected converters," *IEEE Trans. Power Electron*., vol. 27, no. 8, pp. 3467–3471, Aug. 2012.

[8] T. F. Wu, C. L. Kuo, K. H.. Sun, Y. K. Chen, Y. R. Chang and Y. D. Lee, " Integration and operation of a single-phase bidirectional inverter with two buck/boost MPPTs for DC-distribution applications", *IEEE Trans. Power Electron.,* Vol. 28, no. 11, pp. 5098-5106, 2013.

[9] H. Fujita, T. Yamasaki, and H. Akagi, "A hybrid active filter for damping of harmonic resonance in industrial power systems," *IEEE Trans. Power Electron*., vol. 15, no. 2, pp. 215–222, Mar. 2000.

[10] S. Rahmani, A. Hamadi, K. Al-Haddad, and L. A. Dessaint,"A combination of shunt hybrid power filter and thyristor controlled reactor for power quality enhancement," *IEEE Trans. Ind. Electron*., vol. 61, no. 5, pp. 2152–2164,2014.

[11] F. Z. Peng, H. Akagi, and A. Nabae, "A new approach to harmonic compensation in power systems: A combined system of shunt passive and series active filters," *IEEE Trans. Ind. Appl*., vol. 26, no. 6, pp. 983–990, Nov./Dec. 1990.

[12] Choi, Wai-Hei, Chi-Seng Lam, and Man- Chung Wong. "Current compensation and DC-link voltage control for current quality compensator", *Proc. of COMPEL 2012*, 2012.

[13] W. Tangtheerajaroonwong, T. Hatada, K. Wada, and H. Akagi, "Design and performance of a transformerless shunt hybrid filter integrated into a three-phase diode rectifier," *IEEE Trans. Power Electron*., vol. 22, no. 5,pp. 1882–1889, Sep. 2007.

[14] H. Akagi and K. Isozaki, "A hybrid active filter for a three-phase 12-pulse diode rectifier used as the front end of a medium voltage motor drive," *IEEE Trans. .Power Electron*., vol. 27, no. 1, pp. 69–77, 2012.

[15] NingYi Dai, Chi-Seng Lam, and WenChen Zhang, "Multifunctional Voltage Source Inverter for Renewable Energy Integration and Power Quality Conditioning," *The Scientific World Journal*, vol. 2014, 10 pages, 2014. doi:10.1155/2014/421628

[16] A. Luo, Z. K. Shuai, Z. J. Shen, W. J. Zhu, and X. Y. Xu, "Design considerations for maintaining dc-side voltage of hybrid active power filter with injection circuit," *IEEE Trans. Power Electron.*, vol. 24, no. 1,pp. 75–84, Jan. 2009.

[17] Wen-Chen Zhang, Ning-Yi Dai, Man-Chung Wong, Chi-Kong Wong, "Capacitive-coupled grid-connected inverter with active power injection ability", *in Proc. of ECCE (Asia) 2012*, pp. 1-7.

[18] C.-S. Lam, W.-H. Choi, M.-C. Wong, and Y.-D. Han, "Adaptive DC-link voltage-controlled hybrid active power filters for reactive power compensation," *IEEE Trans. Power Electronic*, vol. 27, no. 4, pp. 1758–1772,2012

[19] C.P. Zheng, N.Y.Dai, M. C. Wong, C. K. Wong and M. Zhu, "Capacitive-coupling inverter for PV integration: analysis and implementation", *in Proc. Of ICIEA 2014*, pp. 666-671.

[20] S. Jiang, D. Cao, Y. Li, F. Z. Peng, "Grid-Connected Boost-Half-Bridge Photovoltaic Microinverter System Using Repetitive Current Control and Maximum Power Point Tracking" *IEEE Trans. Power Electron*., Vol. 27, no. 11,pp.4712-4721, Nov. 2012